# Sensorless Fuzzy Direct Torque Control for High Performance Electric Vehicle with Four In-Wheel Motors

**M'hamed Sekour[†], Kada Hartani\*, Azeddine Draou\*\* and Ahmed Allali\*\*\***

**Abstract** – This paper describes a control scheme of speed sensorless fuzzy direct torque control (FDTC) of permanent magnet synchronous motor for electric vehicle (EV). Electric vehicle requires fast torque response and high efficiency of the drive. Speed sensorless FDTC In-wheel PMSM drives without mechanical speed sensors at the motor shaft have the attractions of low cost, quick response and high reliability in electric vehicle application. This paper presents a new approach to estimate the speed of in-wheel electrical vehicles based on Model Reference Adaptive System (MRAS). The direct torque control suffers in low speeds due to the effect of changes in stator resistance on the flux measurements. To improve the system performance at low speeds, a PI-fuzzy resistance estimator is proposed to eliminate the error due to changes in stator resistance. High performance sensorless drive of the in-wheel motor based on MRAS with on line stator resistance tuning is established for four motorized wheels electric vehicle and the whole system is simulated by matalb/simulink. The simulation results show the effectiveness of the new control strategy. This proposed control strategy is extensively used in electric vehicle application.

**Keywords**: Electric vehicle, Fuzzy logic, In-wheel motor, Sensorless control, Model Reference Adaptive system, Direct torque control.

## 1. Introduction

The primary topology of power train system in electric vehicle has not evolved greatly since the emergence of electric vehicles. The conventional electric vehicle has a concentrated power system, which, as illustrated in Fig. 1, has only motor and has to engage a differential to distribute the driving power for the left and the right wheels. Compared with the IC engine vehicle, this type of electric vehicle can be thought of as a simple replacement of the engine by a motor and the gas tank by the battery, which results in extra mechanical parts and more maintenance, and also hinders the performance of motion control implemented in the vehicle. However, the practical use of in-wheel motor (Fig. 2) has allowed for some revolutionary changes in the design of electric vehicle with the introduction of new topologies. In the following century, the technology of in-wheel motors developed continuously. Especially in last several decades, in-wheel motors have been improved dramatically due to rapid developments in power electronics and electromagnetic technology [1, 2] and [3].

Compared with the conventional electric vehicle design with a single motor situated centrally driving two or four wheels by axles (Figs. 1(b) and (c)), the in-wheel motor arrangement has some significant advantages:
- High controllability for all-wheel driving vehicles
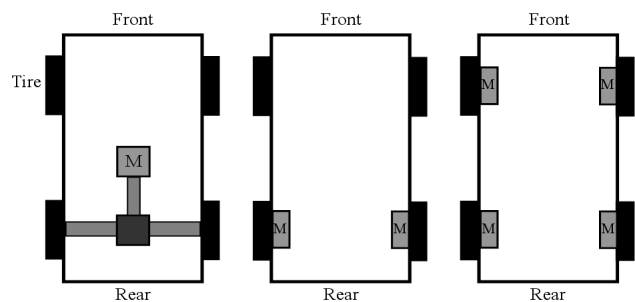- High energy efficiency



**Fig. 1.** Various arrangement of motor drive systems for electric vehicles proposed up to now : (a) A front or rear wheel driven by one motor; (b) Rear wheels driven by in-wheel motors; (c) Four wheels driven by in-wheel motors
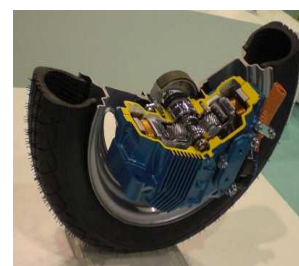


**Fig. 2.** An in-wheel motor

†   Corresponding Author: Electrotechnical Engineering Laboratory, Saida University, Algeria. (mohamed_sekour@yahoo.fr)
\*   Electrotechnical Engineering Laboratory, Saida University, Algeria. (kada_hartani@yahoo.fr)
\*\*  Dept. of Electrical, University of Hail, Kingdom of Saudi Arabia. (adraou@yahoo.com)
\*\*\* Dept. of Electrical Engineering, University of Sciences and Technology of Oran, Algeria. (ahmed.alllali@univ-usto.dz)

- Greater freedom in layout design

Due to the advantages of in-wheel motors, there is no doubt that more and more electric vehicles will adopt the topologies of the powertrain system shown in Figure 3 to make full use of these merits. Therefore, the electric vehicle driven by four in-wheel motors is used in this work.

Electric vehicle is a road vehicle, based on electric propulsion. The electric propulsion system is the heart new generation of EV [4]. It consists of the motor drive, transmission device, and wheels. The motor drive consists of the electric motor, power converter, and electronic controller, which are the core of the EV propulsion system. Traditionally, DC motors have been prominent in electric propulsion because their torque-speed characteristics have suited to traction requirement well and their speed control is simple. Recently, permanent magnet synchronous motors (PMSM) have been extensively analyzed as feasible candidates for variable speed electric vehicle (EV) traction application [5]. The PMSM exhibits high efficiency when operating at constant speed in the constant torque region due to its lower (copper) losses. For improving the dynamic performance of induction motor drives for electric vehicle propulsion, generally vector control techniques is preferred. In recent years an innovative control method called direct torque control (DTC) has gained the attraction for electric propulsion system [6-8], because it can also produce fast torque control of the permanent magnet synchronous motor and does not need heavy computation on-line, in contrast to vector control.

The proposed control structure is based on the sensorless fuzzy direct torque control (FDTC) for each in-wheel motor. The main goal of using a FDTC algorithm for PMSM drives is to overcome some of the drawbacks of the original DTC. However, this reduces torque ripple greatly and the fast response and robustness merits of the classical DTC [9-13] are entirely preserved by eliminating hysteresis regulators of flux and torque.

Sensorless control of permanent magnet synchronous motor drives is now receiving wide attention [15-19]. The main reason is that the speed sensors spoils the ruggedness and simplicity of PMSM. In a hostile environment, speed sensors cannot even mounted.

This paper is organized as follow : First, a four wheel vehicle model is presented. In section 2, a speed sensorless control is proposed. In this case, speed estimation is based on MRAS (Model Reference Adaptive System) method. Especially, it is not very sensitive to the parameters of motor, so MRAS is a widely applicable method and it attracts much attension [15-19]. In section 3, the problems of stator resistance for the fuzzy direct torque controlled permanent magnet synchronous machine drive have been examined. The relationship between the reference current vector and the reference flux and torque has been determined and then used for $R_s$ estimation. A PI-fuzzy compensation method of the $R_s$ variation based on stator

flux has been proposed and verified through modelling and simulation. Simulation results show the effectiveness of the proposed scheme on the steady-state and transient performance of the drive. The proposed estimator does not require rotor position information and hence retains the sensorless nature of fuzzy DTC of PMSM in-wheel motor. Finally, a series of Matlab/Simulink simulation will carried out to evaluate the performance of the proposed sensorless control system on a curved road.

## 2. Structure of Proposed Electric Vehicle

The electric vehicle structure is composed of four permanent magnet synchronous motors (PMSM). They are integrated in the front and rear wheels of vehicle. They are supplied by a battery through DC-AC inverters. The Fig. 3 illustrates the proposed of EV structure which couples the dynamics of vehicle to electrical motorisation.
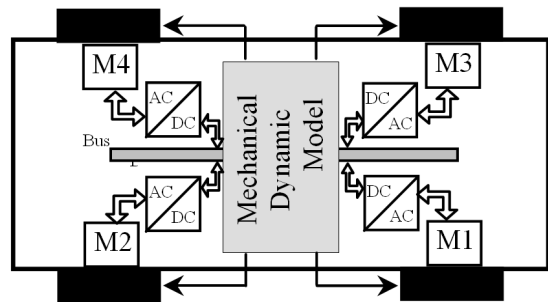


**Fig. 3.** Proposed structure of electric vehicle.

### 2.1 Dynamic model

The dynamic motion of the vehicle is modelled by three equations that represent respectively the longitudinal and lateral translational motion and the yaw rotational movement (Fig. 4) [20]:

$$M_v\ddot{X} = F_X$$
$$M_v\ddot{Y} = F_Y \qquad (1)$$
$$J_v\ddot{\psi} = M_z$$

Where $v_x$ is the longitudinal velocity, $v_y$ is the lateral one, $\dot{\Psi}$ the yaw rate while, $J_v$ the moment of inertia. $F_X$, $F_Y$ and $M_z$ are respectively the total forces acting in $X$ and $Y$ directions and the total yawing moment. They are clearly linked with the velocities in reference frame by the obvious relationship:

$$\begin{pmatrix} \dot{X} \\ \dot{Y} \\ \dot{\Psi} \end{pmatrix} = \begin{pmatrix} \cos(\Psi) & -\sin(\Psi) & 0 \\ \sin(\Psi) & \cos(\Psi) & 0 \\ 0 & 0 & 1 \end{pmatrix} \begin{pmatrix} v_x \\ v_y \\ r \end{pmatrix} \qquad (2)$$
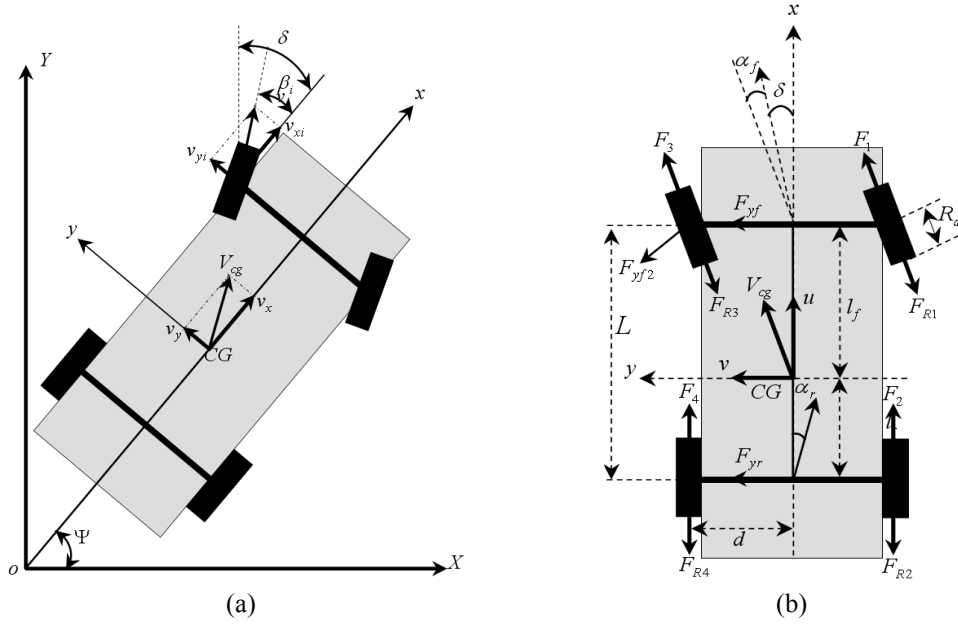
**Fig. 4.** Vehicle model: (a) Reference frame for a rigid vehicle; (b) Directional geometry

Although there are many ways to obtain the mathematical model, a procedure based on Lagrange equations will be followed here; neglecting the relational kinetic energy of the wheels the kinetic energy of the vehicle is as follows:

$$T = \frac{1}{2} M_v \left( \dot{X}^2 + \dot{Y}^2 \right) + \frac{1}{2} J_v \dot{\psi}^2 \qquad (3)$$

and the equations of motion can be obtained by the relation :

$$\frac{d}{dt} \left( \frac{\partial T}{\partial \dot{q}_i} \right) - \frac{\partial T}{\partial q_i} = Q_i \qquad (4)$$

where the coordinates $q_i$ are $X$, $Y$ and $\Psi$, and $Q_i$ are the corresponding forces $F_X$, $F_Y$ and $M_z$.

Performing the relevant derivatives with respect to time and introducing forces $F_X$ and $F_Y$ written with reference to vehicle frame, we obtain:

$$\begin{aligned} F_x &= M_v \left( \dot{v}_x - r v_y \right) \\ F_y &= M_v \left( \dot{v}_y + r v_y \right) \\ M_z &= J_v \dot{r} \end{aligned} \qquad (5)$$

Using a linear tire model, the front and rear cornering forces can be expressed as the product of the cornering stiffness ($C_f$, $C_r$) by the sideslip angle ($\alpha_f$, $\alpha_r$)

$$\begin{aligned} F_{yf} &= -C_f \alpha_f \\ F_{yr} &= -C_r \alpha_r \end{aligned} \qquad (6)$$

The sideslip angles of the wheels can be expressed easily in terms of the longitudinal, lateral, angular velocities and the steering angle $\delta$. The explicit expressions of the sideslip angles for the front and rear axles are represented in Eq. (7).

$$\begin{aligned} \alpha_f &= \tan^{-1} \left( \frac{v_y + l_f r}{v_x} \right) - \delta \\ \alpha_r &= \tan^{-1} \left( \frac{v_y - l_r r}{v_x} \right) \end{aligned} \qquad (7)$$

We can obtain the three governing equations of motion by finding the resultant of forces acting on vehicle in $x$, $y$ directions and the total yawing moment about the center of gravity CG, then substituting in the system of equations (equation 5) with taken in consedation the cornering forces and the sideslip angles. The longitudinal, lateral and angular accelerations of vehicle are represented as follow.

$$\dot{v}_x = v_y r + \frac{F_{t1} + F_{t2} + F_{t3} + F_{t4} - F_{res}}{M_v} + \frac{C_f \delta}{M_v} \left( \frac{v_y + r l_r}{v_x} - \delta \right)$$

$$\dot{v}_y = \left( -\frac{C_r + C_f}{M_v v_x} \right) v_y + \left( \frac{C_r l_r + C_f l_f}{M_v v_x} - v_x \right) r + \frac{C_f}{M_v} \delta$$

$$\dot{r} = \left( \frac{C_r l_r - C_f l_f}{J_v v_x} \right) v_y - \left( \frac{C_r l_r^2 + C_f l_f^2}{J_v v_x} \right) r$$

$$+ \frac{C_f l_f}{J_v} \delta + \frac{d}{J_v} \left( F_{t1} + F_{t2} - F_{t3} - F_{t4} \right) \qquad (8)$$

Where $F_{t1}$, $F_{t2}$, $F_{t3}$, $F_{t4}$ are the tractive forces of motors, $F_{res}$ is the resistant forces which including the

aerodynamic drag force $F_{aero}$, climbing force $F_c$ and rolling force $F_{rr}$. They have the following expressions [21]:

$$F_{aero} = \frac{1}{2} \rho S_f C_{px} V_{cg}^2$$
$$F_c = M_v g \sin(\alpha_p) \qquad (9)$$
$$F_{rr} = C_{rr} M_v g$$

By applying a driving force to a tire which has a certain slip ($\lambda$), the longitudinal coefficient ($\mu$) is influenced by the wheel sideslip angle ($\alpha_f$, $\alpha_r$). Moreover, the longitudinal slip can be defined for the four wheels as:

$$\lambda_i = \frac{R_\omega \omega_i - u_{ti}}{\max(R_\omega \omega_i, u_{ti})}, \quad i \in [1,...,4] \qquad (10)$$

Where $R_\omega$ is the wheel radius, $\omega$ is the angular velocity of the in-wheel motor and $u_t$ is the linear speed at which the contact zone moves on the ground and can be written for the four wheels as [21]:

$$u_{t1} = (v_x + dr)\cos(\delta) + (v_y + l_f r)\sin(\delta)$$
$$u_{t2} = v_x + dr$$
$$u_{t3} = (v_x - dr)\cos(\delta) + (v_y + l_f r)\sin(\delta) \qquad (11)$$
$$u_{t4} = v_x - dr$$

The "Magic Formul" is used to describe the longitudinal road/tire interaction, namely the relationship between slip ratio $\lambda$ and traction coefficient $\mu$ [20-22]. In the Pacejka's magic model, the normalized traction force (i.e. $\mu$) between tire and road is medeled as:

$$\mu = c_1 \left( \sin\left( c_2 \tan^{-1} \left( c_3 \lambda - c_4 \left( c_3 \lambda - \tan^{-1}(c_3 \lambda) \right) \right) \right) \right) \qquad (12)$$

Coefficient sets of $c_1$, $c_2$, $c_3$ and $c_4$ used for simulating various road surface are shown in Table 1.

**Table 1.** The friction model coefficients

| Surface | $c_1$ | $c_2$ | $c_3$ | $c_4$ |
|---------|-------|-------|-------|-------|
| Normal | 1 | 1,9 | 10 | 0,97 |
| Wet | 0,82 | 2,3 | 12 | 1 |
| Snow | 0,3 | 2 | 5 | 1 |
| Ice | 0,1 | 2 | 4 | 1 |

The longitudinal force for the four in-wheel motors can be calculated by the next equation:

$$F_{ti} = \frac{g M_v}{4} \mu_i \cos(\alpha_p), \quad i \in [1,...,4] \qquad (13)$$

The drive system model can be described by the following mechanical equations:

$$T_{ri} = F_{ti} R_\omega - N_f d_z \qquad , i \in [1,3]$$
$$T_{ri} = F_{ti} R_\omega - N_r d_z \qquad , i \in [2,4] \qquad (14)$$

Where $T_{ri}$ is the resistance torque $N_f, N_r$ are the front and rear normal force have the following expressions:

$$N_f = \frac{M_v g}{2} \left( \frac{l_r}{L} - \frac{h_{cg}}{L_g} \frac{dV_{cg}}{dt} \alpha_p - \frac{h_{cg}}{L} \alpha_p \right)$$
$$N_r = \frac{M_v g}{2} \left( \frac{l_f}{L} + \frac{h_{cg}}{L_g} \frac{dV_{cg}}{dt} \alpha_p + \frac{h_{cg}}{L} \alpha_p \right) \qquad (15)$$

## 3. Sensorless Fuzzy DTC with PI Fuzzy Stator Resistance Estimator

The fuzzy direct torque control uses the stator flux amplitude and the electromagnetic torque errors through two fuzzy logic controllers to generate a voltage space vector (reference voltage) by acting on both the amplitude and the angle of its components, which is used by a space vector modulation to provide the inverter switching states. The mamdani's and sugeno methods are used for the fuzzy reasoning algorithms in the two fuzzy logic controllers [7].

### 3.1 PI-fuzzy stator resistance estimator

With Fuzzy DTC, the electromagnetic torque and stator flux can be estimated using the measured stator voltages and currents. The estimation does not depend on motor parameters except for the stator resistance. The variation of stator resistance due to change on temperature or frequency degrade the performance of fuzzy DTC controlled by introducing errors in the estimated flux linkage vector and the electromagnetic torque. Compensation for the effect of stator resistance variation then become necessary. Estimation of the stator resistance and its compensation using a PI-fuzzy estimator has been proposed in this section.

The block diagram of PI-Fuzzy stator resistance compensator is shown in Fig. 6. The error in the stator flux linkage is used as an input to the PI-Fuzzy estimator. The technique is based on the principle that the change in stator resistance will cause a change in stator current and stator flux linkage $\Phi_s$. The error between the stator flux linkage $\Phi_s$ and its reference $\Phi_s^*$ is propotional to the stator resistance change.

The equation for PI resistance is given by:

$$\Delta R_s = \left( k_p + k_i \frac{Tz}{z-1} \right) \Delta \Phi_s \qquad (16)$$

Where $T$ is the sampling time, $k_p$ and $k_i$ are the proportional and integral gains of the PI estimator, $\Delta R_s$ is the change in the stator resistance.
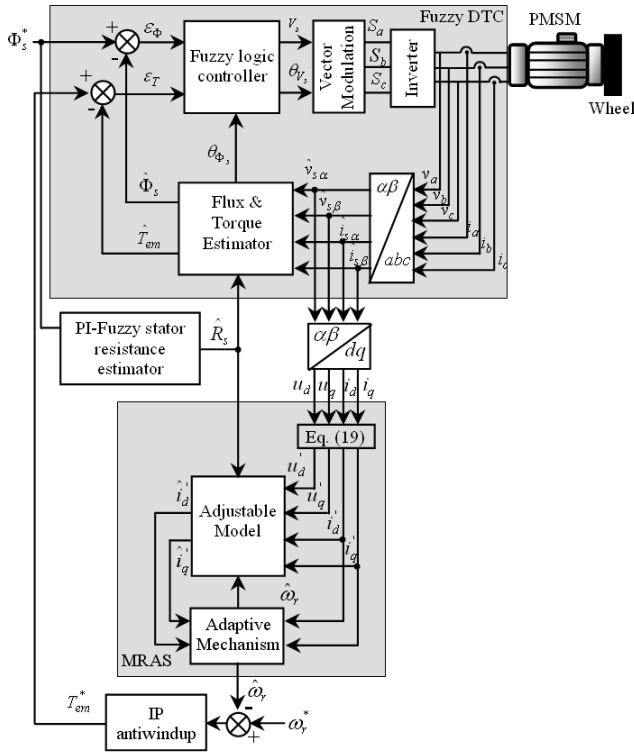
**Fig. 5.** Sensorless fuzzy DTC scheme with PI-fuzzy stator resistance estimator
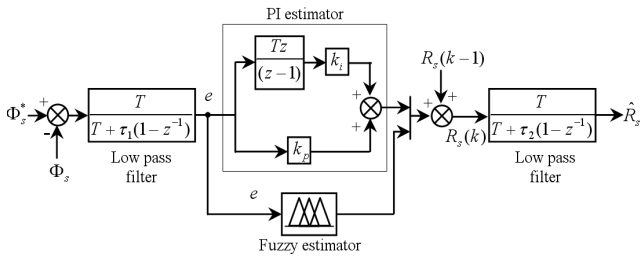


**Fig. 6.** PI-Fuzzy stator resistance estimator

The error between the estimated stator $\Phi_s$ and its reference $\Phi_s^*$ is passed through a low pass filter with a very low cuttof frequency in order to attenuate stator flux. Then the signal is passed through a PI-Fuzzy estimator. The output of the PI-Fuzzy estimator is the required change of resistance $\Delta R_s$ due to change in temperature or frequency. The change of stator resistance $\Delta R_s$ is continuously added to the previously estimates stator resistance $R_s(k-1)$. The final estimated stator resistance $R_s(k)$ can used directly in the controller [26].

To study the performance of the PI-Fuzzy resistance estimator with sensorless fuzzy direct torque control strategy, the simulation was conducted using Matlab/Simulink. Figs. 7 and 8 show the simulation results for a step stator resistance change for uncompensated and compensated system respectively.

In actual operating conditions, the rate of change of temperature is quite slow. A linear changing stator resistance
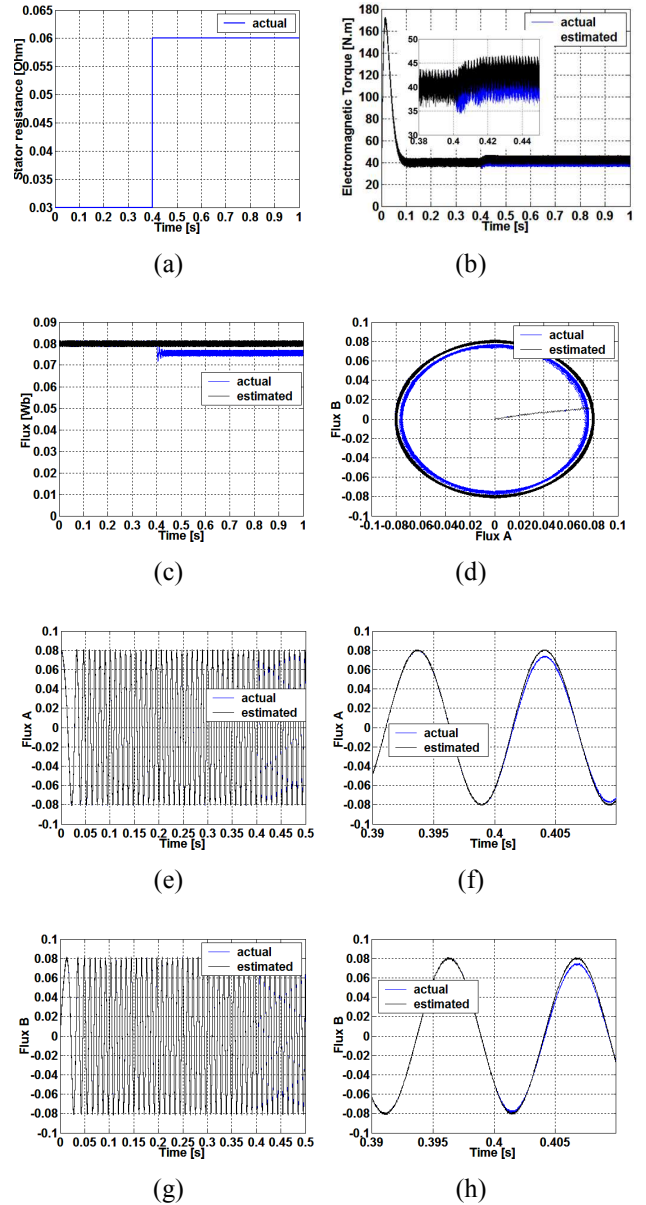


**Fig. 7.** Response due to step stator resistance change (un-compensated)

was modeled. Fig. 7 shows the torque and flux responses when the stator resistance changes as indicated by Fig. 7(a). It is seen that the stator flux and the torque deviate from their reference values. These deviations may cause the Fuzzy DTC drive system to become unstable.

The PI-Fuzzy estimator of Fig. 6 was incorporated into sensorless Fuzzy DTC system as indicated by Fig. 5. Fig. 8 shows the tracking performance of the estimator to the actual change in $R_s$. The estimation error is approximately 0.025%, as in Fig. 8(b). Fig. 8 shows the torque and flux response of the sensorless DTC for an abrupt change in $R_s$ when stator resistance changes as indicated in Fig. 8(a). It is seen from Figs. 8(c) and (d) that the torque and stator flux are constant with the PI-fuzzy resistance estimator.
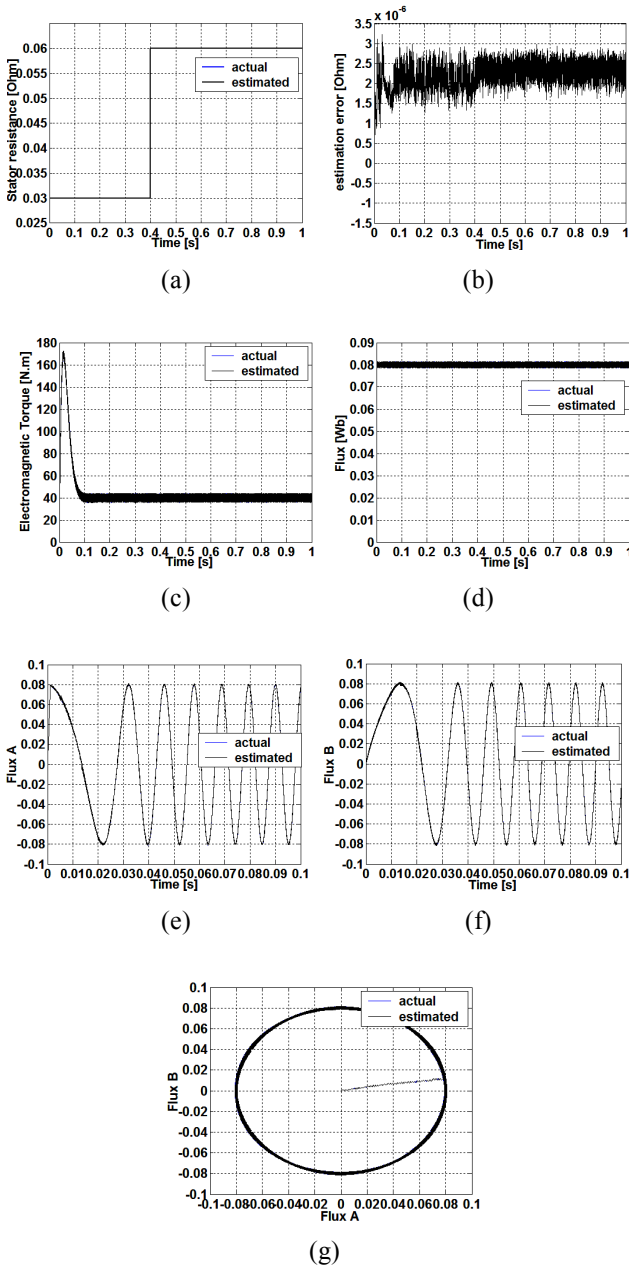
(a)



(b)



(c)



(d)



(e)



(f)



(g)

**Fig. 8** Response due to step stator resistance change (compensated)

### 3.1 Sensorless control system based on MRAS

The MRAS sensorless control is based on the motor current model in the rotating $dq$ frame, Fig. 5.

$$\frac{d}{dt}\begin{bmatrix} i_d' \\ i_q' \end{bmatrix} = \begin{bmatrix} -\dfrac{R_s}{L_d} & \dfrac{\omega_r L_q}{L_d} \\ -\dfrac{\omega_r L_d}{L_q} & -\dfrac{R_s}{L_q} \end{bmatrix}\begin{bmatrix} i_d' \\ i_q' \end{bmatrix} + \begin{bmatrix} \dfrac{1}{L_d} & 0 \\ 0 & \dfrac{1}{L_q} \end{bmatrix}\begin{bmatrix} v_d' \\ v_q' \end{bmatrix} \quad (17)$$

Where

$$\begin{cases} i_d' = i_d + \dfrac{\Phi_f}{L_d} \\ i_q' = i_q \\ v_d' = v_d + \dfrac{R_s \Phi_f}{L_d} \\ v_q' = v_q \end{cases} \quad (18)$$

According to the PMSM current model described by Eq. (17), the estimation model can be obtained and can be expressed as follows:

$$\frac{d}{dt}\begin{bmatrix} \hat{i}_d' \\ \hat{i}_q' \end{bmatrix} = \begin{bmatrix} -\dfrac{\hat{R}_s}{L_d} & \dfrac{\hat{\omega}_r L_q}{L_d} \\ -\dfrac{\hat{\omega}_r L_d}{L_q} & -\dfrac{\hat{R}_s}{L_q} \end{bmatrix}\begin{bmatrix} \hat{i}_d' \\ \hat{i}_q' \end{bmatrix} + \begin{bmatrix} \dfrac{1}{L_d} & 0 \\ 0 & \dfrac{1}{L_q} \end{bmatrix}\begin{bmatrix} v_d' \\ v_q' \end{bmatrix} \quad (19)$$

Where $\hat{i}_d'$ and $\hat{i}_q'$ are the estimated value of equivalent $dq$ axis currents respectively, and $\hat{\omega}_r$ is the estimated value of electrical rotor speed.

According to the classical theory of MRAS, there should be two models including a reference model and an adjustable model. In this paper, the motor is the reference model and the current model of the PMSM (described by Eq. (19)) is the adjustable model. The estimated value of rotor rotating speed $\hat{\omega}_r$ will converge to the true value $\omega_r$ through an appropriate adaptive mechanism.

In this process, the most critical work is to get a suitable adaptive mechanism and ensure the stability of the system. If we define a generalized error $e$, the equation of the generalized error will be obtained by extracting Eq. (19) from Eq. (18) :

$$\frac{de}{dt} = Ae - W \quad (20)$$

Where :

$$A = \begin{bmatrix} -\dfrac{R_s}{L_d} & \dfrac{\omega_r L_q}{L_d} \\ -\dfrac{\omega_r L_d}{L_q} & -\dfrac{R_s}{L_q} \end{bmatrix}, \quad J = \begin{bmatrix} 0 & \dfrac{L_q}{L_d} \\ -\dfrac{L_d}{L_q} & 0 \end{bmatrix},$$

$$e = \begin{bmatrix} e_d \\ e_q \end{bmatrix} = i_s' - \hat{i}_s', \quad i_s' = \begin{bmatrix} i_d' \\ i_q' \end{bmatrix} \quad \hat{i}_s' = \begin{bmatrix} \hat{i}_d' \\ \hat{i}_q' \end{bmatrix},$$

$$W = J(\hat{\omega}_r - \omega_r)\hat{i}_s'$$

Because, the mechanical time constant is must greater than electrical time constant, the parameter $\omega_r$ in matrix $A$ can be considered as a time invariant parameter in the digital control system. Then, it is easy to find that the system described by Eq. (20) is a standard nonliear time-

varying feedback system. So Popov's hyperstability theory based on the standard feedback system can be utilized to design the adaptive mechanism. In order to describe the system as a complete standard feedback system, Eq. (22) is transformed to Eq. (21):

$$\begin{cases} \dfrac{de}{dt} = Ae - IW \\ v = De \end{cases} \qquad (21)$$

Choose $D = I$, then $v = e$.

According to hyperstability theory, as a stability condition, the Popov integral inequality [12] described by (22) must be fulfilled:

$$\eta(0, t_1) = \int_0^{t_1} v^T W dt \geq -\gamma_0^2, \quad \forall t_1 \geq 0 \qquad (22)$$

Where $\gamma_0$ is a limited positive number.

In this control system, the Popov integral inequality is specifically described by inequality (23).

$$\begin{aligned} \eta(0, t_1) &= \int_0^{t_1} v^T W dt \\ &= \int_0^{t_1} \left( \frac{L_q}{L_d} \hat{i}_q' e_d - \frac{L_d}{L_q} \hat{i}_d' e_q \right) (\hat{\omega}_r - \omega_r) dt \geq -\gamma_0^2 \end{aligned} \qquad (23)$$

As the adjustable parameter $\hat{\omega}_r$ which has converged to the real parameter $\omega_r$ in reference model is necessary to direct torque control, there should be "memory" in adaptive mechanism. Then the integrator can be adopted and $\hat{\omega}_r$ can be assumed as follow :

$$\hat{\omega}_r = \int_0^t \Gamma_\omega(e) d\tau + +\hat{\omega}_r(0) \qquad (24)$$

Where $\Gamma_\omega(e)$ is an expression relative to generalized error $e$. Then the inequality (22) will transform to inequality (24).

$$\begin{aligned} \eta(0, t_1) &= \int_0^{t_1} \left( \frac{L_q}{L_d} \hat{i}_q' e_d - \frac{L_d}{L_q} \hat{i}_d' e_q \right) \times \dots \\ &\times \left( \int_0^t \Gamma_\omega(e) d\tau + \hat{\omega}_r(0) - \omega_r \right) dt \geq -\gamma_0^2 \end{aligned} \qquad (25)$$

In order to obtain suitable $\Gamma_\omega(e)$, an integral inequality which is well known can be utilized, and ti is shnown as inequality (26).

$$\int_0^{t_1} \frac{df(t)}{dt} kf(t) dt = \frac{k}{2} \left[ f^2(t_1) - f^2(0) \right] \geq -\frac{1}{2} kf^2(0) \\ (k > 0) \qquad (26)$$

According to the inequality (27), it is easy to make assumptions described by Eqs. (27) and (28).

$$\frac{df}{dt} = \frac{L_q}{L_d} \hat{i}_q' e_d - \frac{L_d}{L_q} \hat{i}_d' e_q \qquad (27)$$

$$kf(t) = \int_0^t \Gamma_\omega(e) d\tau + \hat{\omega}_r(0) - \omega_r \qquad (28)$$

Where $f(t)$ is a function for the use of derivation, $\hat{\omega}_r(0)$ is initial estimated rotor speed. Then the derivation from Eq. (27) will be obtained :

$$\Phi_\omega(e) = k \left( \frac{L_q}{L_d} \hat{i}_q' e_d - \frac{L_d}{L_q} \hat{i}_d' e_q \right) \quad (k > 0) \qquad (29)$$

Therefore the estimated speed will be obtained by combining Eqs. (24) and (29):

$$\begin{aligned} \hat{\omega}_r &= \int_0^t k \left( \frac{L_q}{L_d} \hat{i}_q' e_d - \frac{L_d}{L_q} \hat{i}_d' e_q \right) d\tau + \hat{\omega}_r(0) \\ &= \frac{k}{s} \left[ -\frac{L_q}{L_d} \left( i_q' - \hat{i}_q' \right) \hat{i}_d' + \frac{L_d}{L_q} \left( i_d' - \hat{i}_d' \right) \hat{i}_q' \right] + \hat{\omega}_r(0) \end{aligned} \qquad (30)$$

In order to improve the dynamic performance, the proportional regulation can be added into the adaptive mechanism [12]. Finally the adaptive mechanism is a PI regulator shown by Eq. (31).

$$\hat{\omega}_r = \left( k_p + \frac{k_i}{s} \right) \left[ -\frac{L_q}{L_d} \left( i_q' - \hat{i}_q' \right) \hat{i}_d' + \frac{L_d}{L_q} \left( i_d' - \hat{i}_d' \right) \hat{i}_q' \right] + \hat{\omega}_r(0) \qquad (31)$$

To estimate the position of rotor, the integral operation is performed as :

$$\hat{\theta} = \int \hat{\omega}_r dt \qquad (32)$$

We illustrate in Figs. 9-11 and 12 the steady-state responses of the sensorless (drive) fuzzy DTC PMSM drive under full load condition at a speed of 600rd/s. In Fig. 9, the reference, estimated and actual speed signals are shown in red, black and blue respectively. The estimated and reference torque and flux signals are shown in Figs. 11 and Fig. 12 respectively. We can assert that the MRAS observer tracks the actual speed very well and the estimation error is very small, Fig. 10.
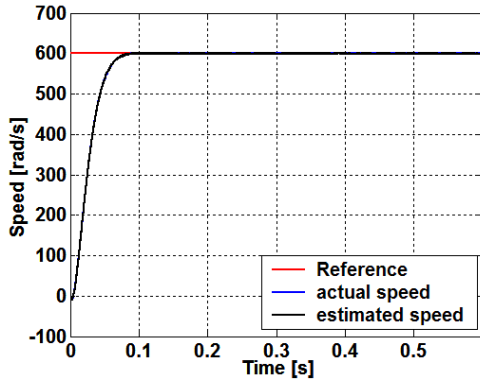
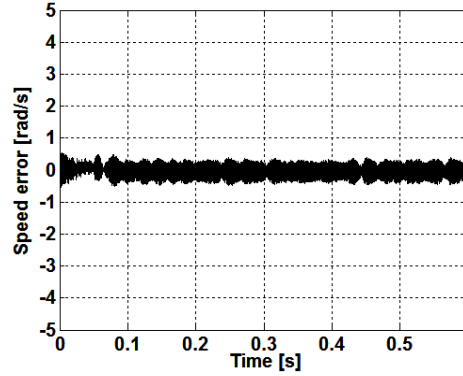**Fig. 9.** Estimated and actual speed



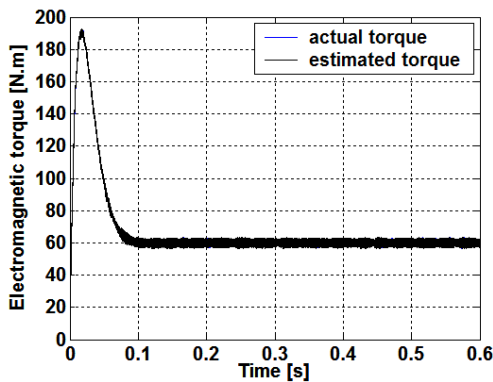**Fig. 10.** The error of estimated speed



**Fig. 11.** Estimated and actual electromagnetic torque
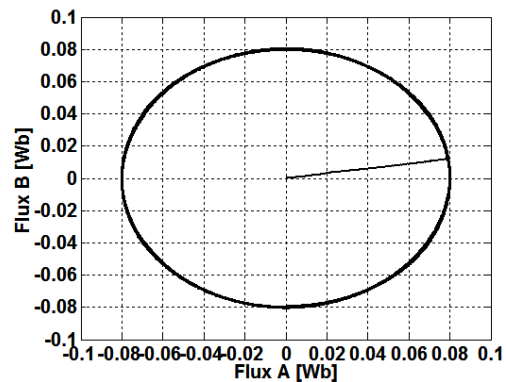


**Fig. 12.** Stator flux

## 4. Simulation results

In this study, a simulation model of a three degree-of-freedom model of the vehicle is presented in order to evaluate the effectiveness of the proposed control system. The proposed system uses the vehicle speed, the slope angle and the steering angle as input parameters and calculates the required inner and outer speeds. The four motors are controlled by a fuzzy direct torque control through an inverter supplied by DC voltage source $E$ of 510 (volt). Table 2 summarizes the vehicle characteristics and parameter numerical values. The parameters of the PMSMs are given in Table 3.

Fig. 13 shows the dynamical model of the considered electric vehicle with a four in-wheel motors' topology that was numerically implemented on Matlab / Simulink. This scheme consists of a block capable of representing the different dynamics of the vehicle which has the steering angle $\delta$, the slope angle $\alpha_p$ and the rotational speeds of the motors ($\omega_1, \omega_2, \omega_3, \omega_4$) as inputs. Basically, it is responsible of calculating the longitudinal, lateral and angular velocity of the vehicle from the traction forces generated by the four motors. In the block called Slip, we can estimate the longitudinal slip ($s_1, s_2, s_3, s_4$), calculate the side slip angles ($\alpha_1, \alpha_2, \alpha_3, \alpha_4$), and the loads on each wheel ($N_1, N_2, N_3, N_4$). Moreover, we can
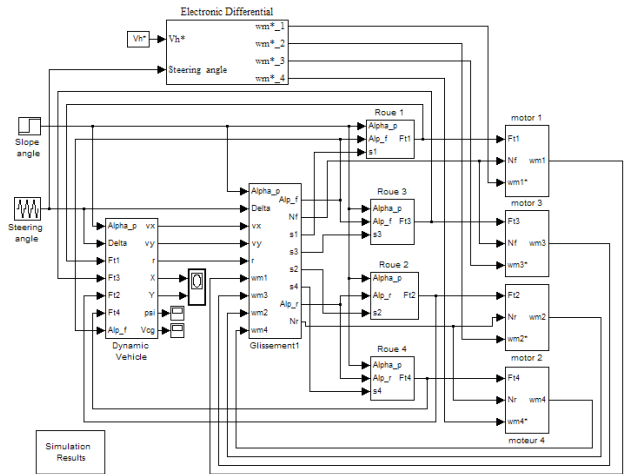


**Fig. 13.** Simulink model of the electric vehicle

calculate the traction forces in the blocks (Wheel 1, Wheel 2, Wheel 3, Wheel 4) by determining the longitudinal coefficient from the inputs to the blocks. The four blocks representing the four motors use the inputs to estimate the load torques required to produce the corresponding rotational speed. Finally, the block named Electronic differential provides the difference of speed for the four-wheel drives while the vehicle is performing a turn, which

will result on (a better) the best stability of vehicle in the curved trajectory of the road, and for various conditions of the environment. When the steering angle is equal to zero, the electric vehicle drives on the straight road and the electronic differential does not need to work (intervene). On the other hand, if the steering angle changes, it indicates that the vehicle is making a turn and the electronic differential begins to work (be part of the speed control system involving 4 drives). The common reference speed $\omega^*$ is then set by the accelerator pedal command. The actual reference speeds for the left drives ($\omega_3^*$, $\omega_4^*$) and the right drives ($\omega_1^*$, $\omega_2^*$) can then be obtained (defined) by adjusting the common reference speed $\omega^*$ using the output signal of the steering angle block.

The vehicle speed starts from zero to the chosen reference speed. At this operating point, two turns, one to the left and one to the right are imposed to the vehicle chassis by the steering angle. Fig. 14 shows the steering angle in which the maximum value is (7°). The vehicle turns to the left at $t = 12s$, and when the steering angle reaches its maximum value at $t = 15s$, and still be maintained at the mentioned value about 5 seconds and then it is brought to zero at $t = 23s$. After that, the vehicle is steered towards the right from the instant of $t = 27s$ for a period of 11 seconds before being put back to its trajectory at the instant $t = 38s$. The sensorless fuzzy direct torque control (FDTC) based strategy imposed on each motor-wheel system is also applied to the four-wheel drive.
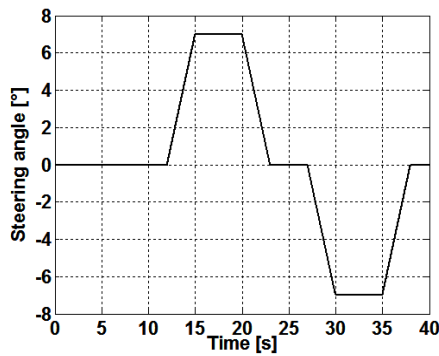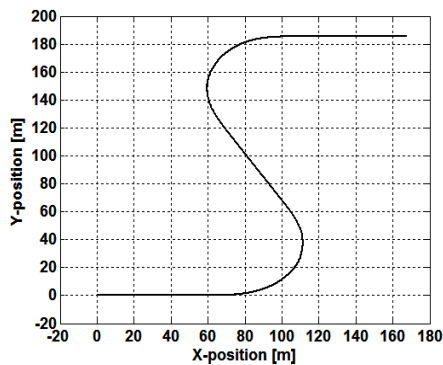
Fig. 15 shows the trajectory traced out by the vehicle. It is clearly shown that the vehicle starts from rest and continues on its linear path until the steering angle starts to rise by imposing a left turn at first. Then, a turning to the right causes the vehicle to change its direction, and thus continues its journey until the end of the simulation time.

Fig. 16(a) shows the longitudinal velocity of the vehicle $v_x$. We notice a dissipation of energy due to the lateral sliding. This dissipation is reflected by a slight decrease on the speed when the vehicle is cornering as reported in Fig. 16(b). In fact we can notice a slight decrease when the driver applies a steering.

As for the lateral velocity $v_y$ and the yaw moment $r$, we can immediately recognize that their existence depends solely on the steering angle reference as shown in Fig. 17 and Fig. 18. We can clearly see that these two speeds occur
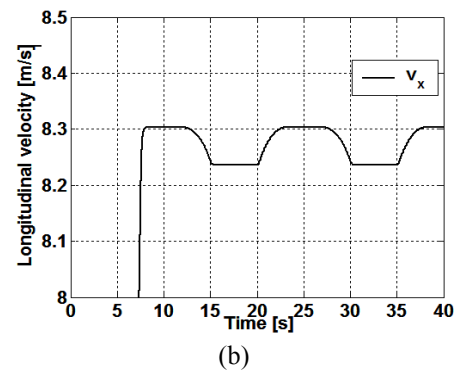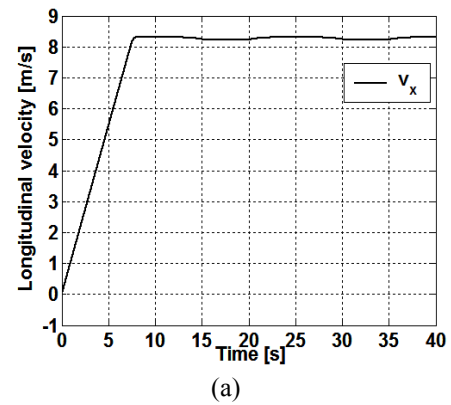


(a)



**Fig. 14.** Steering angle

(b)

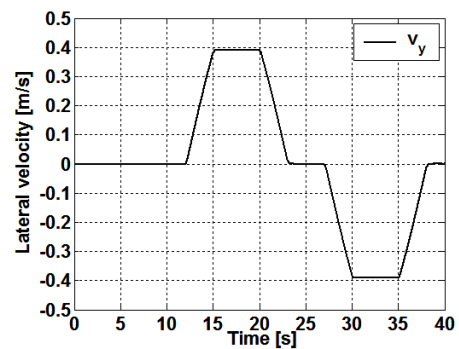**Fig. 16.** Longitudinal velocity



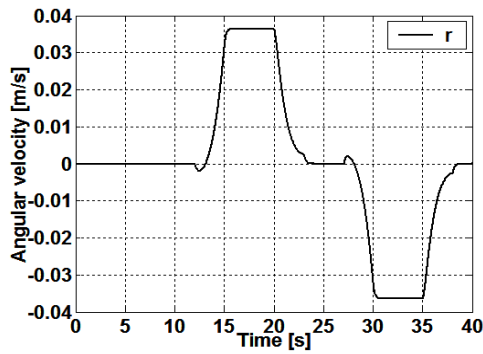**Fig. 15.** Vehicle path



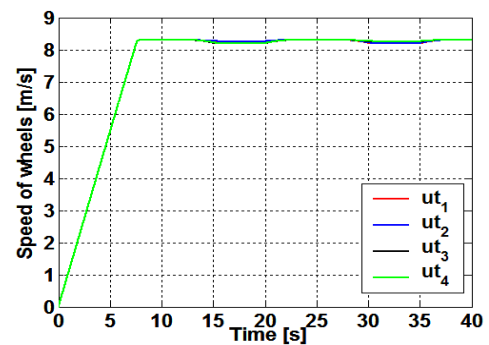**Fig. 17.** Lateral velocity

**Fig. 18.** Angular velocity
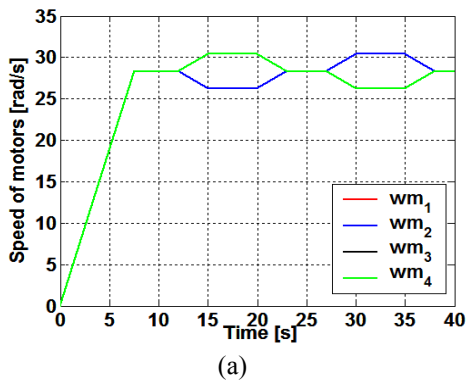


(a)
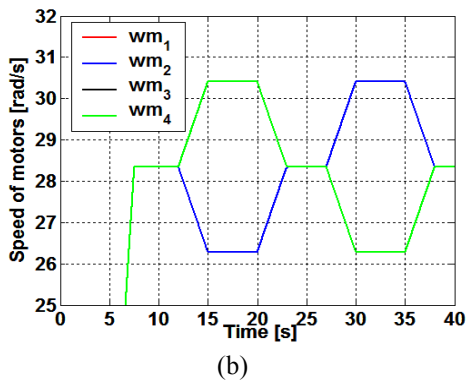


(b)

**Fig. 19.** Rotational speed of motors

outside the turn. At that time, the speeds of the wheels change values which will have an immediate impact on the electrical and mechanical quantities. During the first steering, the motors (M1 and M2) located outside of the turn's curvature, rotate at higher speeds than motors (M3 and M4). On the other hand, we can notice that the motors (M3 and M4) rotate at higher speeds than the motors (M1 and M2) during the second steering as can be seen in Fig. 19 (b).

Fig. 20 depicts the linear speed of wheels. A good tracking of the longitudinal velocity of the vehicle can be observed. In fact, we can notice also a slight decrease when the driver applies a steering. However, similar responses could be noticed for the speeds of the 4 driving wheels of the vehicle, as shown in Fig. 16.



(a)



(b)

**Fig. 20.** Speed of wheels

only during cornering and they vanish when the vehicle is traveling on a straight road. It is interesting to note that the lateral and angular speeds of the vehicle keep the same waveform compared to the steering angle, and only their amplitudes vary.
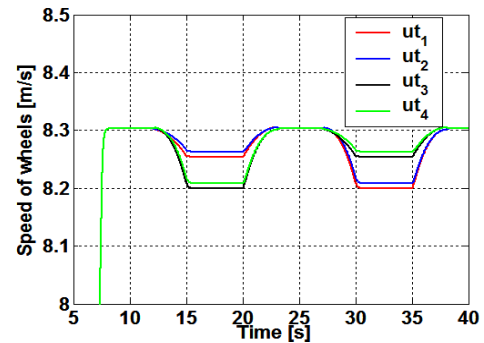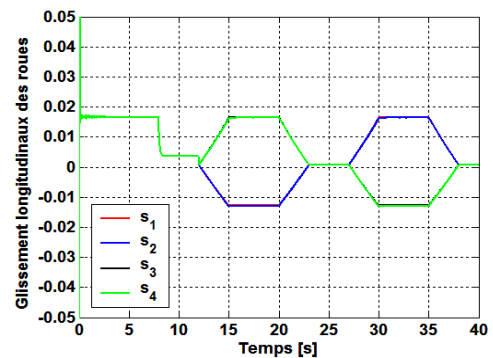
Fig. 19 (a) shows the estimated rotational speeds of the motors. We notice that they have the same speed variations from the start up to the establishment of the steady state speeds as long as the vehicle runs on a straight path. We suppose that the turns are made at a constant speed, the driver gives a steering angle that begins to be a steering angle of the guiding wheels (front wheels). The electronic differential acts immediately on the four motors simultaneously, lowering the speed of the wheels that are located inside the turn, on the contrary of those located
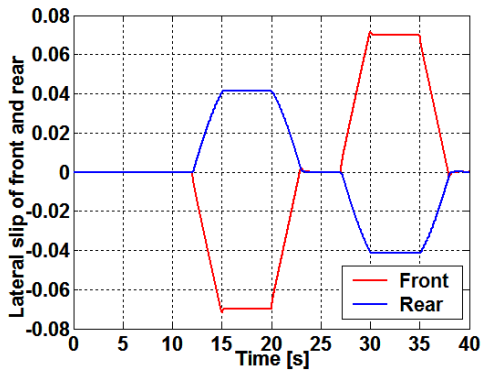


**Fig. 21.** Longitudinal slip of wheels

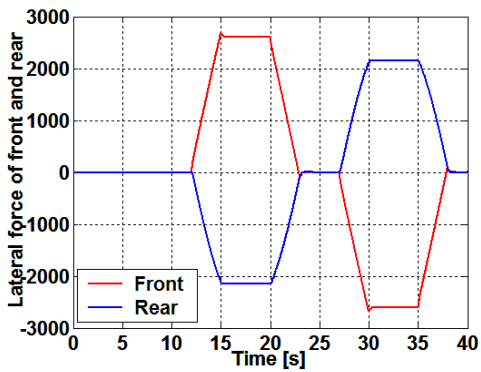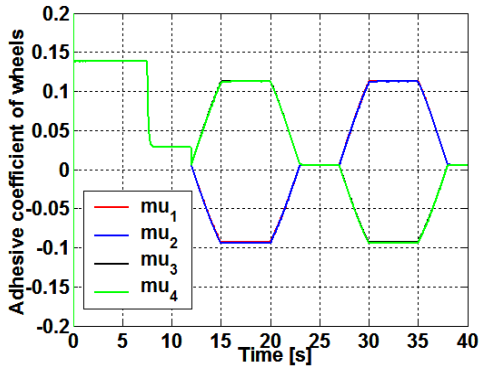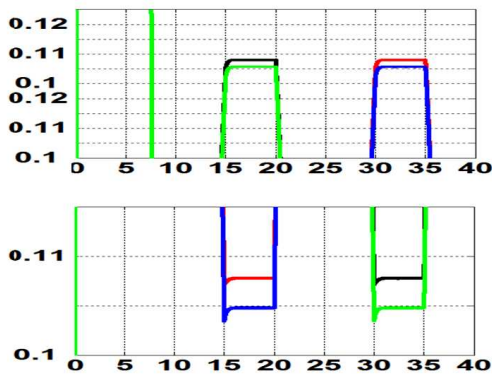**Fig. 22.** Lateral slip of front and rear wheels



**Fig. 23.** Lateral force of front and rear wheels



(a)



(b)

**Fig. 24.** Adhesive coefficient of wheels

The behaviour of the lateral slip of wheels is illustrated by Fig. 21. We should note that the longitudinal slips ($s_1$, $s_2$, $s_3$, $s_4$) of four wheels are maintained in the adhesive region.

The lateral side slip of front and rear wheels are shown in Fig. 22, as well.

The variation of the lateral force of front and rear wheels are shown in Fig. 23. As shown in this figure and during the turn trajectory of the vehicle, the lateral force applied to both front and rear driving wheels show different values.

It can be observed in Fig. 24, that the adhesive coefficient of the outer driven wheels is bigger than those of the inner one. Therefore, the stability is maintained during the vehicle turn.

Fig. 25 illustrates the traction forces generated by the motors of the front axle (M1 and M3) and the two motors of the rear axle (M2 and M4). First, we notice high traction forces are provided by the motors for moving the vehicle from startup. This seems logical since these forces must overcome the overall resisting forces to the movement of the vehicle. Moreover, we may also report a discrepancy between the traction forces during the movement through a turn. Indeed, the motors located within the curvature of the turn produce lower traction forces than those of the motors that are outside the curvature of the turn. This scheme also applies to the load torques imposed on the motors as can be seen in Fig. 26.

Fig. 25 shows the difference in the traction forces of motors during the completion of a turn. This can also be
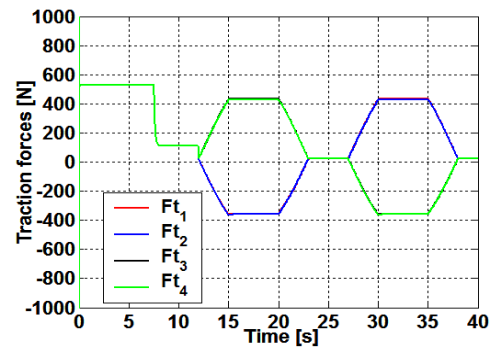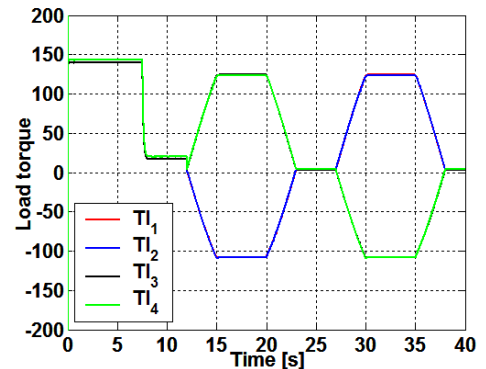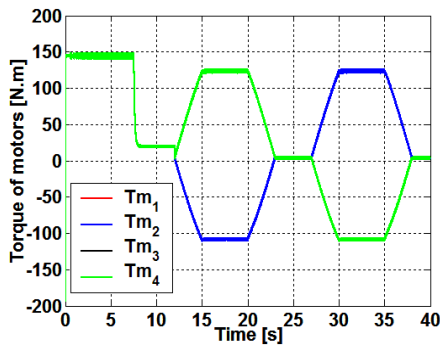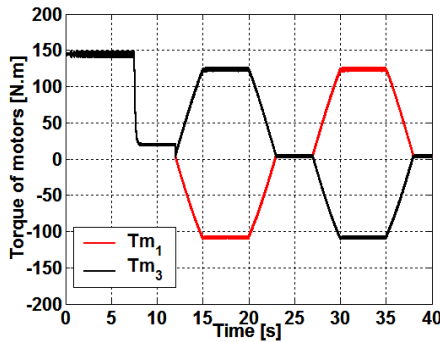


**Fig. 25.** Traction forces



**Fig. 26.** Resistive torque

(a)



(b)



(c)

**Fig. 27.** Torque of motors





**Fig. 28.** Phase currents of the motors (M1 and M3)

clearly seen for the speed of motors (Fig. 19) and the resistant torque of motors (Fig. 26). When the speeds of motors on the left side and right side diverge, the left wheels slow down and the right wheels speed up to traverse the turn.

Fig. 27 (a) illustrates the variation of the electromagnetic torque of the motors. We have first, a high torque during the start up, the motors maintain these high electromagnetic torques from start up until the time their stabilized speeds are reached. At this time, the motor torques begin to decrease and then stabilize at a certain set point. We can also notice a discrepancy between the motor torques each time it passes through a turn. The electromagnetic torques developed by the motors (M3 and M4) are higher than those of the motors (M1 and M2) at the first turn but
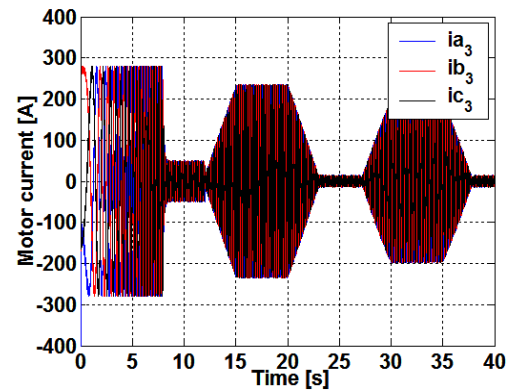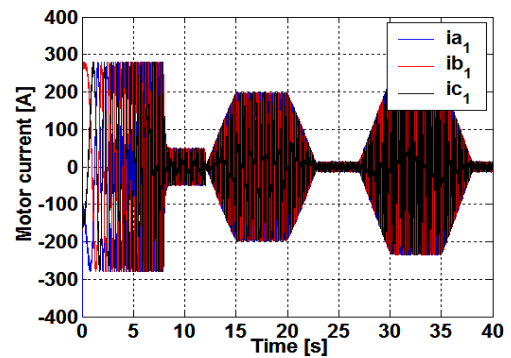
during the second turn, the opposite is verified as can be clearly seen in Figs. 27 (b) and Fig. 27 (c). It can be observed that the torques of the outer motors are greater than that of the inner ones.

The phase currents variations of the motors (M1 and M3) are illustrated in Figs. 28 (a) and (b).

## 5. Conclusion

In this paper, a new technique improving the sensorless control performances for in-wheel electrical vehicles under stator resistance uncertainties is proposed. A PI-fuzzy stator resistance compensator is designed and applied to eliminate the effect of stator resistance variation in sensorless fuzzy DTC controlled in-wheel electrical vehicles. The performance of PI-fuzzy estimator is verified by modelling based on Matlab/Simulink. These studies show that the PI-fuzzy stator resistance estimator is capable of tracking the stator resistance very well and can also overcome the problem of instability caused by a large mismatch between the controlled and the actual stator resistance. The sensorless control was carried out on in-wheel based on MRAS method. The simulation results exhibit good performance of control in dynamic and steady state. A three-degree freedom vehicle model was employed in the simulation. The proposed sensorless control system on a curved road can significantly improve vehicle handling performance.

## Appendix

**Table A.1** The specifications of the vehicle used in simulation

| | | |
|---|---|---|
| $M_v$ | Vehicle mass | 1562 kg |
| $J_v$ | Vehicle inertia | 2630 kg.m² |
| $J_\omega$ | Wheel inertia | 1,284 kg.m² |
| $L_f$ | Distance from the CG to front axle | 1,104 m |
| $L_r$ | Distance from the CG to rear axle | 1,421 m |
| $h_{cg}$ | Heigh of the vehicle ctroid (CG) | 0,5 m |
| $S_f$ | Frontal area of vehicle | 2,04 m² |
| $\rho$ | Air density | 1,2 kg.m⁻³ |
| $C_{px}$ | Drag coefficient | 0,25 |
| $C_{rr}$ | Rolling resistance coefficient | 0,01 |
| $C_f$ | Longitudinal stiffness of each tire lateral | 37407 N/rad |
| $C_r$ | Lateral stiffness of each tire lateral | 51918 N/rad |
| $R_\omega$ | Wheel radius | 0,294 m |

**Table A.2** The specifications of motors

| | | |
|---|---|---|
| $R_s$ | Resistance | 0,03  $\Omega$ |
| $L_s$ | Inductance | 0,2 mH |
| $\Phi_f$ | Permanent magnet flux | 0,08 Wb |
| $p$ | Pole pairs | 4 |

## References

[1] L. Chunhua, K. T. Chau, J. Z. Jiang, "A permanent magnet hybrid in-wheel motor drive for electric vehicles", *Proceeding of IEEE Vehicle Power and Propulsion Conference,* 2008.

[2] A. Goodazi, E. Esmailzadeh, "Design of a VDC system for all-wheel independent drive vehicles", *IEEE/ASME Transactions on Mechanics,* Vol. 12, No. 6, pp. 632-639, 2007.

[3] T. Masayuki, A. Tadashi, M. Takayuki, N. Kazuo, F. Noboru, Y. Masayuki, "Novel motors and controllers for high performance electric vehicle with Four in-wheel motors", *IEEE Transactions on Industrial Electronics,* Vol. 44, No. 1, pp. 28-38, 1997.

[4] C. Chan, "The state of the art of electric and hybrid vehicles", *Proc. Of the IEEE,* Vol. 90, No. 2, pp. 247-275, Feb. 2002.

[5] M. A. Rahman, R. Qin, "A permanent magnet hysteresis hybrid synchronous motor for electric vehicles", *IEEE Trans. Ind. Electron.* Vol. 44, No. 1, pp. 46-53, Feb. 1997.

[6] Kada Hartani, Yahia Miloud, "Vehicle Stability Enhancement Control for Electric Vehicle Using Behaviour Model Control", *Book : Electric Vehicles - Modelling and Simulations*, ISBN 978-953-307-477-1, Edited by: Seref Soylu, Publisher: InTech, Chapter 6, p. 127-158, September 2011.

[7] K. Hartani, Y. Miloud, A. Miloudi "Improved Direct Torque Control of Permanent Magnet Synchronous Electrical Vehicle Motor with Proportional-Integral Resistance Estimator", *Journal of Electrical Engineering & Technology*, Vol. 5, N°3, pp. 451-461, September 2010.

[8] Kada Hartani, Mohamed Bourahla, Yahia Miloud, Mohamed Sekour, "Electronic Differential with Direct Torque Fuzzy Control for Vehicle Propulsion System", *Turkish Journal of Electrical Engineering & Computer Sciences,* Vol. 17, N°1, pp. 21-38, March 2009.

[9] Takahachi and T. Noguchi, "A new quick-response and high-efficiency control strategy of an induction motor", *IEEE Trans. Ind. Applicat.,* Vol. 22, No. 5, pp. 820-827, 1986.

[10] T.J. Vyncke, J. A. Melkebeek, and R. K. Boel, "Direct torque control of permanent magnet synchronous motors - an overview", *in conf.Proc. 3$^{rd}$ IEEE Benelux Young Research Symposium in Electrical Power Engineering,* No. 28, Ghent, Begium, Apr. 27-28, p.5, 2006.

[11] D. Casadei, G. Serra, A. Tani, "Implementation of direct torque control algorithm for induction motors based on discrt space vector modulation", *IEEE Trans. on Power Electronics.* Vol. 15, No. 4, pp. 769-777, July 2000.

[12] C. French, P. Acarnley, "Direct torque control of permanent magnet drives", *IEEE Trans. Ind. Appl.* Vol. 32, No. 5, pp. 1080-1088, Sep./Oct. 1996.

[13] B. Hredzak, S., Gair, J. F., Eastham,"Elimination of torque pulsations in a direct drive EV wheel motor", *IEEE Trans.actions Magn.* Vol. 32, No. 5, pp. 5010-5012, Sep. 1996.

[14] A. Goodazi, E. Esmailzadeh, "Design of a VDC system for all-wheel independent drive vehicles", *IEEE/ASME Transactions on Mechanics,* Vol. 12, No. 6, pp. 632-639, 2007.

[15] Young Sam, K. Kyoon Kim, K. Young Ahn, 'MRAS based senrorless control for permanent magnet synchronous motor", *SICE Annual Conference in Fukui,* August 4-6, pp. 1632-1637, 2003.

[16] Y. Ruzhong, L. Beizhi, F. Zhou, "Sensorless control of PMSMs based on parameter optimized MRAS speed observer", *Proceeding of the IEEE International Conference on Automation and Logistics Qingdao*, China, pp. 1573-1578, September 2008.

[17] X. Xiaodong, H. Yikang, "Sensorless operation of PMSM vased on Hybrid rotor position self-sensing scheme", *Proceeding of International Conference on Electrical Machines and Systems*, Seoul Korea, pp. 714-718, October 8-11, 2007.

[18] W. Hao, Z. Deng, X. Wang, "Enhanced Adaptive Observer for sensorless PMSM drive system", *Trans-*

*actions of China Electrotechnical Society*, Vol. 24, No. 3, pp. 41-46, March 2009.

[19] X. Xiao, Y. Li, M. Zhang, Y. Liang, "A sensorless control based on MRAS method in interior permanent magnet machine drive", *PEDS,* pp. 734-738, 2005.

[20] G. Genta, "Motor vehicle dynamics: modeling and simulation", *Series on Advances in Mathematics for Applied Sciences*. World Scientific Publishing Co. Pte. Ltd, Vol. 43, 1997.

[21] E. Esmailzadeh, G. R. Vossoghi, A. Goodarzi, "Dynamic modeling and analysis of a four motorized wheels vehicle", *Vehicle System Dynamics*, Vol. 35, pp. 163-194, 2001.

[22] H. B. Pacejk, "Tire and Vehicle dynamics", Second edition, Butterworth-Heinemann, pp. 165-166, 2006.

[23] E. Bakker, H.B. Pacejka, L. Lidner, "A new tire model with an application in vehicle dynamics studies", SAE paper, 1989.

[24] U. Kiencke, L. Nielsen, "Automotive control system", 2000.

[25] Stephant, A. Charar, D. Meizel, "Force model comparaison on the wheel-ground contact for vehicle dynamics", *IEEE Intelligent Vehicle Symposium,* Versailles, June 2002.

[26] S. Mir, M. E. Elbuluk and D. S. Zinger, "PI and Fuzzy Estimators for Tuning the stator resistance in direct torque control of induction machines"*,* IEEE Transactions Power Electronics, Vol. 13, No. 2, pp. 279-287, March, 1998.

is an associate professor at university of Saida. His fields of interest include: multimachines multiconverters systems, Antilock brake system, Traction control system, Anti-skid control for electric vehicle. . e-mail: kada_hartani@yahoo.fr



**Azeddine Draou** was born in Maghnia, Algeria . He received the B.Eng degree from Sheffield University, UK in 1980, the M.Sc degree from Aston University in Birmingham, UK in 1981, and the Ph.D degree from Tokyo Institute of Technology, Japan in 1994 all in Electrical Engineering. From 1982 to 1986 he was a senior Engineer for Sonatrach Ammonia plant, Arzew, Algeria. In 1986, he joined the department of Electrotechnics at the university of Sciences and Technology of Oran, Algeria as a lecturer. He was promoted to Assistant Professor in 1989, Associate Professor in 1996. He is now on leave from his university. He has published over 100 papers in technical journals and conference proceedings. He has also co-authored in the "Power Electronics Handbook" edited by Dr. M.H.Rashid, with Academic Press in 2001. He received the IEE Japan medal for the 1994 annual meeting. His main area of research includes power electronics, static VAR compensation, multilevel inverters, intelligent control of AC drives, UPFC and FACTS devices.
Dr. Draou is a Senior member of the IEEE/ P.E.S, I.E.S, I.A.S societies since 2002. e-mail: adraou@yahoo.com



**M'hamed Sekour** was born in Saida (Algeria) in1964. He obtained a diploma of engineer in Electrotechnic in in 1989 from the University of ENSET Oran (Algeria). He received his master at University of ENSET Oran (Algeria) from 2006 at 2008. He is now an associate professor at university of Saida. His main research interests are in the field of the analysis and intelligent control of electrical machines, multimachines multiconverters systems, modeling and simulation of Fuzzy controllers and vehicular technology. e-mail: mohamed_sekour@yahoo.fr



**Kada Hartani** was born in Saida (Algeria) in 1976. He obtained a diploma of engineer in Electrotechnic in 1997. He received his master at University of Sciences and Technology of Oran (Algeria) from 2001 at 2003. He received "Doctorat Es-Science" in Electrical Control from the University of Sciences and Technology of Oran (Algeria) in 2007. He



**Ahmed Allali** was born on 03.07.1960 in Mecheria Naama Algeria. In 1987 he graduated at the Electrotechnical Department of the Faculty of Electrical Engineering at University (USTO) in Algeria. He defended his "Magister". In the field of optimal power flow problems in 1990; his thesis title was "Optimal Distribution of Active Powers Using Linear Programming with Losses Cost Minimization", and the PhD degree from in 2006; His scientific research is focusing a control and real time simulation of power systems, and study of the Dynamic stability of the networks electrical supply. Actually he is interested in power electronics in particular to the facts and in renewable energies (wind and solar energy). He is currently Professor of electrical engineering at The University of USTO (Algeria) e-mail: allalia@yahoo.com